ACS APPLIED MATERIALS & INTERFACES
Research Article
www.acsami.org

WO_3 and W Thermal Atomic Layer Etching Using "Conversion-Fluorination" and "Oxidation-Conversion-Fluorination" Mechanisms

Nicholas R. Johnson[†] and Steven M. George[*,†,‡]

[†]Department of Chemistry and Biochemistry, and [‡]Department of Mechanical Engineering, University of Colorado, Boulder, Colorado 80309, United States

ABSTRACT: The thermal atomic layer etching (ALE) of WO_3 and W was demonstrated with new "conversion-fluorination" and "oxidation-conversion-fluorination" etching mechanisms. Both of these mechanisms are based on sequential, self-limiting reactions. WO_3 ALE was achieved by a "conversion-fluorination" mechanism using an AB exposure sequence with boron trichloride (BCl_3) and hydrogen fluoride (HF). BCl_3 converts the WO_3 surface to a B_2O_3 layer while forming volatile WO_xCl_y products. Subsequently, HF spontaneously etches the B_2O_3 layer producing volatile BF_3 and H_2O products. In situ spectroscopic ellipsometry (SE) studies determined that the BCl_3 and HF reactions were self-limiting versus exposure. The WO_3 ALE etch rates increased with temperature from 0.55 Å/cycle at 128 °C to 4.19 Å/cycle at 207 °C. W served as an etch stop because BCl_3 and HF could not etch the underlying W film. W ALE was performed using a three-step "oxidation-conversion-fluorination" mechanism. In this ABC exposure sequence, the W surface is first oxidized to a WO_3 layer using O_2/O_3. Subsequently, the WO_3 layer is etched with BCl_3 and HF. SE could simultaneously monitor the W and WO_3 thicknesses and conversion of W to WO_3. SE measurements showed that the W film thickness decreased linearly with number of ABC reaction cycles. W ALE was shown to be self-limiting with respect to each reaction in the ABC process. The etch rate for W ALE was ~2.5 Å/cycle at 207 °C. An oxide thickness of ~20 Å remained after W ALE, but could be removed by sequential BCl_3 and HF exposures without affecting the W layer. These new etching mechanisms will enable the thermal ALE of a variety of additional metal materials including those that have volatile metal fluorides.

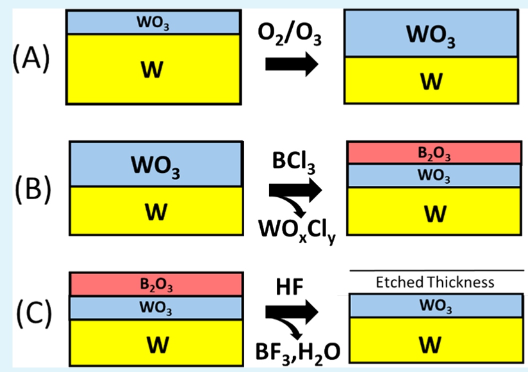

KEYWORDS: *etching, atomic layer etching, WO_3, W, oxidation, fluorination, conversion*

1. INTRODUCTION

The continued miniaturization of advanced semiconductor devices requires atomic layer control in both growth and etching processes.[1] Atomic layer deposition (ALD) and atomic layer etching (ALE) techniques can provide the necessary atomic level precision.[2] ALD techniques have been developed for a wide range of materials over the past few decades and have been extensively adapted by the semiconductor industry.[3,4] In contrast, the need for ALE techniques has emerged more recently, and ALE methods are still in an early stage of development.[5]

Initial plasma ALE methods have been based on surface activation by halogenation followed by ion bombardment to remove surface material.[5] Plasma processes have been developed for a variety of materials including Si,[6,7] compound semiconductors,[8,9] metal oxides,[10−12] and carbon materials.[13,14] The plasma ALE method can achieve anisotropic etching. Thermal ALE techniques have also been demonstrated with fluorination and ligand-exchange reactions.[15] Thermal ALE methods have been developed for Al_2O_3,[16−19] HfO_2,[20] ZrO_2,[21] AlN,[22] and AlF_3.[23] Thermal ALE is able to provide isotropic etching.

Materials with volatile metal fluorides do not have thermal ALE pathways using fluorination and ligand-exchange reactions because their fluorides are gases. Other materials, such as elemental metals, may fluorinate readily and produce fluoride layers too thick for ALE. For these materials, alternative pathways are required for controlled atomic layer etching. Some new strategies in thermal ALE have recently been introduced based on "conversion-etch" mechanisms.[24,25] In the conversion-etch procedure, the surface layer is converted to a different material that can be fluorinated and removed by ligand-exchange. Conversion-etch approaches also have the potential to provide pathways for the ALE of materials with volatile fluorides.

In this Article, "conversion-fluorination" and "oxidation-conversion-fluorination" mechanisms are demonstrated for thermal ALE. The conversion reactions utilize BCl_3 as the reactant. BCl_3 has the ability to convert many metal oxides to B_2O_3. B_2O_3 has a volatile fluoride and can be easily removed spontaneously as BF_3 and H_2O by HF exposures. The example of "conversion-fluorination" is WO_3 ALE using BCl_3 and HF as the reactants in an AB sequence. The example of "oxidation-

Received: June 26, 2017
Accepted: September 6, 2017
Published: September 6, 2017

DOI: 10.1021/acsami.7b09161
ACS Appl. Mater. Interfaces 2017, 9, 34435−34447

conversion-fluorination" is W ALE using O_2/O_3, BCl_3, and HF in an ABC sequence.

Figure 1 shows the various reaction steps for W and WO_3 ALE. In reaction A, W is oxidized to WO_3 using ozone (O_2/O_3). In reaction B, BCl_3 is used to convert the surface of WO_3 to a B_2O_3 surface layer. During this conversion, the chlorine ligands are transferred from BCl_3 to the surface to form volatile WO_xCl_y products. In reaction C, the B_2O_3 surface layer can then be etched spontaneously by HF to form H_2O and BF_3 products. The conversion of WO_3 to B_2O_3 is necessary because HF cannot spontaneously etch WO_3.

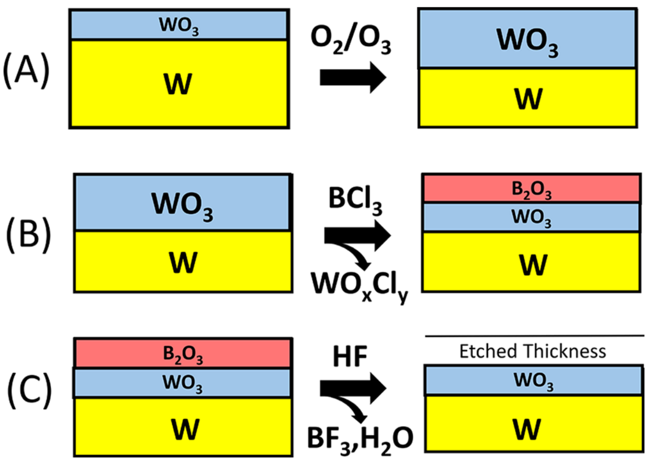

Figure 1. Oxidation, conversion, and fluorination reactions: (A) oxidation of W using O_2/O_3; (B) conversion of W to WO_3 using BCl_3; and (C) fluorination of B_2O_3 by HF to form volatile BF_3 and H_2O.

Reactions A, B, and C in Figure 1 based on oxidation, conversion, and fluorination are all thermochemically favorable.[26] The reaction and standard free energy changes for the oxidation of W to WO_3 using O_3 or O_2 are

$$W + 3O_3(g) \rightarrow WO_3 + 3O_2(g)$$
$$\Delta G°(200\ °C) = -296.7\ \text{kcal/mol} \quad (1)$$

$$W + 3/2O_2(g) \rightarrow WO_3$$
$$\Delta G°(200\ °C) = -171.7\ \text{kcal/mol} \quad (2)$$

Proposed conversion reactions of WO_3 with BCl_3 to yield various possible WO_xCl_y reaction products and their standard free energy changes are

$$WO_3 + 2BCl_3(g) \rightarrow B_2O_3 + WCl_6(g)$$
$$\Delta G°(200\ °C) = -7.7\ \text{kcal/mol} \quad (3)$$

$$WO_3 + 4/3BCl_3(g) \rightarrow 2/3B_2O_3 + WOCl_4(g)$$
$$\Delta G°(200\ °C) = -4.3\ \text{kcal/mol} \quad (4)$$

$$WO_3 + 2/3BCl_3(g) \rightarrow 1/3B_2O_3 + WO_2Cl_2(g)$$
$$\Delta G°(200\ °C) = -7.8\ \text{kcal/mol} \quad (5)$$

In addition, the reaction for the fluorination of B_2O_3 to volatile BF_3 and H_2O reaction products and the standard free energy change is

$$B_2O_3 + 6HF(g) \rightarrow 2BF_3(g) + 3H_2O(g)$$
$$\Delta G°(200\ °C) = -17.3\ \text{kcal/mol} \quad (6)$$

After removal of the B_2O_3 surface layer, a new W or WO_3 surface remains. The reactions can then be repeated to etch either W or WO_3. W ALE uses reactions A, B, and C. WO_3 ALE uses reactions B and C.

HF alone should not etch or react with the WO_3 or W surface. Likewise, BCl_3 should not react with the W surface. The expectations for these reactions are based on their positive standard free energy changes:

$$WO_3 + 6HF(g) \rightarrow WF_6 + 3H_2O(g)$$
$$\Delta G°(200\ °C) = +32.6\ \text{kcal/mol} \quad (7)$$

$$W + 6HF(g) \rightarrow WF_6(g) + 3H_2(g)$$
$$\Delta G°(200\ °C) = +19.0\ \text{kcal/mol} \quad (8)$$

$$W + 2BCl_3(g) \rightarrow 2B + WCl_6(g)$$
$$\Delta G°(200\ °C) = +95.0\ \text{kcal/mol} \quad (9)$$

W and WO_3 can also be etched spontaneously using various dry etching techniques. Methods for spontaneous tungsten etching utilize plasmas containing various halogens such as fluorine[27−29] or chlorine.[28,30,31] Tungsten etching occurs through formation of volatile chlorides or fluorides. Tungsten can also be etched by Cl_2 or XeF_2 gases.[30,32,33] WO_3 can be etched spontaneously with halogen-containing plasmas using NF_3 or SF_6.[34−36] WF_6 is also known to etch WO_3 spontaneously at >180 °C from WO_3 ALD studies using WF_6 and H_2O as the reactants.[37,38] This spontaneous etching of WO_3 by WF_6 suggests a pathway for W ALE based on sequential reactions with W oxidation followed by WF_6 exposures to remove WO_3.

W ALE and WO_3 ALE may have applications in a variety of areas. In the semiconductor industry, W is employed as a conductor in contact holes and vias.[39] W is also utilized for fabricating gates in 3D NAND memory devices.[40] Outside the semiconductor industry, W has application in MEMS and NEMS structures.[41,42] WO_3 also is a useful material for water splitting[43] and gas sensing.[44] The atomic layer controlled etching of W and WO_3 may be needed for device fabrication. The isotropic etching of W may be particularly useful for the lateral etching required to fabricate W gates in 3D NAND flash memory.[40]

2. EXPERIMENTAL SECTION

W samples were deposited on Si wafers with a 500 nm thermal oxide layer. The SiO_2 layer improves the sensitivity of the in situ spectroscopic ellipsometry (SE) analysis by providing interference enhancement.[45] Al_2O_3 ALD films were first grown on the SiO_2 thermal oxide layer at 130 °C using 15 Al_2O_3 ALD cycles. These Al_2O_3 ALD films provided an adhesion layer for W ALD growth.[46] W ALD films with a thickness of 250 Å were then deposited at 130 °C with sequential self-limiting reactions of WF_6 and Si_2H_6.[47] These Al_2O_3 ALD and W ALD films were deposited in a separate hot-wall viscous flow reactor. Upon exposure to atmosphere, an oxide thickness of 12−30 Å is formed on the W film as determined by X-ray photoelectron spectroscopy (XPS) and X-ray reflectivity (XRR) analysis.[48,49]

The Si wafer was then diced to produce W coupons with dimensions of 1.6 × 1.6 cm. These W coupons were placed in a reaction chamber that has been described previously.[50] This reaction chamber is similar to other plasma atomic layer deposition (ALD)

DOI: 10.1021/acsami.7b09161
ACS Appl. Mater. Interfaces 2017, 9, 34435−34447

reactors equipped for in situ SE measurements.[51] The chamber walls were coated with ~500 cycles of Al_2O_3 ALD using $Al(CH_3)_3$ and H_2O as the reactants at the chamber wall temperature of 170 °C. WO_3 films were prepared by the oxidation of the W ALD films at 280 °C using an O_2 plasma at 600 W with an O_2 pressure of 100 mTorr. The O_2 plasma exposures produced a WO_3 film thickness of 130−150 Å on the W ALD films.

A remote inductively coupled plasma (ICP) provided oxygen radicals for the oxidation of W to WO_3. A quartz tube (6 cm inner diameter × 25 cm long) encircled by a helical copper coil was the ICP source. A 13.56 MHz RF generator (Paramount RF Power Supply, Advanced Energy) and 50 Ω impedance matching network (Navigator Digital Matching Network, Advanced Energy) were used in conjunction to generate the ICP plasma. The distance between the ICP source and the W coupon was ~4 cm.

Etching of the WO_3 and W films was monitored by in situ SE using a J.A. Woollam M-2000D ellipsometer. This ellipsometer has a spectral range of 240−1700 nm and utilized an incidence angle of 70°. The WO_3 and W films were analyzed to obtain film thicknesses after each reaction cycle or each individual reaction. A schematic showing the film stack and ellipsometer optical beams is shown in Figure 2. Note

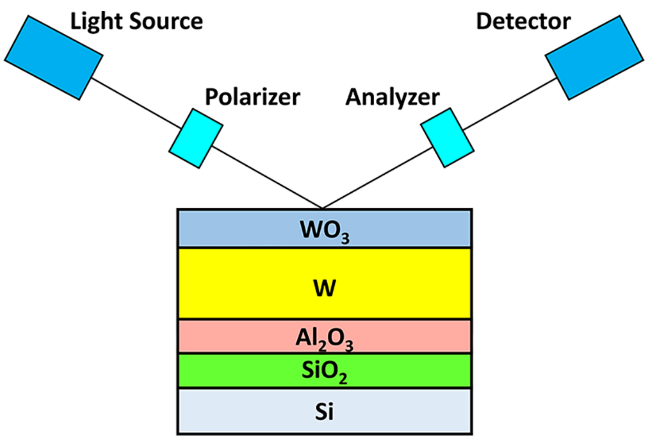

Figure 2. Schematic showing ellipsometer beam interacting with film stack comprised of WO_3, W, Al_2O_3, SiO_2, and underlying Si substrate.

that the individual layer thicknesses are not to scale. SE has the ability to measure the thicknesses of each individual layer in the film stack. This allows for simultaneous determination of the WO_3 and W film thicknesses.

The WO_3 films were analyzed using the Complete Ease software package from J.A. Woollam. The model employed a Tauc−Lorentz oscillator and a Gaussian oscillator.[52] Only the parameters of the Tauc−Lorentz oscillator model were varied from the starting parameters to increase the accuracy of the model. The metal W layer underneath the WO_3 layer was measured by a B-Spline model.[53] n and k values for bulk W were used as the initial parameters and were varied to fit the experimental data.

Boron trichloride (99.9%, Synquest Laboratories) and HF-pyridine (70 wt % HF, Sigma-Aldrich) were used as the reactants. The reactants were separately dosed into the reaction chamber together with a constant stream of ultrahigh purity (UHP) nitrogen. The reactants were introduced using two pneumatic valves (Swagelok-HBVVCR4-C for BCl_3 or Swagelok-6LVV-DPFR4-P-C for HF) on either side of a conductance limiting valve (Swagelok SS-4BMG-VCR). The pneumatic valves were actuated using LabView.

Between each reactant exposure, the reaction chamber was purged with UHP nitrogen gas for 130 s at a pressure of 1180 mTorr. The O_3 for the oxidation reaction during W ALE was produced by an O3ONIA ozone generator with oxygen [Airgas, 99.999%]. The gas flow from the ozone generator contained ~10% of O_3 in O_2. The O_2 pressure used for the oxidation reaction was 70 mTorr. Therefore, the O_3 pressure was ~7 mTorr. The HF and BCl_3 purge times were 130 s during W ALE using the O_2/O_3 exposures. The purge time after the O_2/O_3 exposures was 60 s.

Samples were heated on a sample stage inside of the reaction chamber. A constant temperature of 207 °C was used for all of the ALE experiments performed to determine the self-limiting conditions. The temperature was initially targeted to be 200 °C. A temperature calibration revealed that the temperature was 207 °C. The temperature of the sample stage was varied during the studies of WO_3 ALE etch rate versus temperature. The chamber walls were held constant at 170 °C. A rotary vane pump (Alcatel 2010) was used to pump the chamber to a base pressure of ~20 mTorr. A capacitance monometer measured the chamber base pressure and pressure transients from each reactant.

3. RESULTS AND DISCUSSION

3.1. WO_3 ALE Using "Conversion-Fluorination" with BCl_3 and HF. Figure 3 shows the WO_3 layer thickness

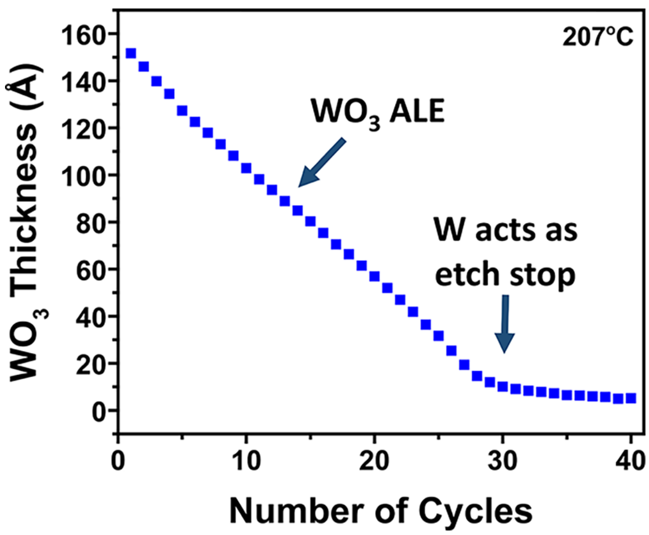

Figure 3. WO_3 thickness versus number of cycles showing WO_3 ALE at 207 °C using BCl_3 and HF as reactants. W film under WO_3 layer acts as an etch stop.

measured using in situ SE during the etching of the WO_3 layer on the W film. These results were obtained using an AB exposure sequence with BCl_3 and HF as the reactants. Figure 3 displays results for 40 reaction cycles at a substrate temperature at 207 °C. The initial WO_3 film thickness is ~150 Å. The WO_3 film thickness decreases linearly until reaching a WO_3 film thickness of ~10 Å. The etching of the WO_3 layer is linear over this range of thicknesses with an etch rate of 4.18 Å/cycle. The SE measurements confirmed that there was no change in the underlying W film thickness during WO_3 etching.

The WO_3 etch rate is reduced dramatically when the WO_3 layer reaches a thickness of ~10 Å. At this point, the WO_3/W interface is nearby and the WO_3 layer may undergo a transition to WO_x oxides where $x < 3$ before reaching the underlying W film. These WO_x oxides may not be amenable to the "conversion-etch" procedure using BCl_3 and HF. As a result, the etch rate slows when the tungsten oxide layer thickness reaches a thickness of ~5 Å. The underlying W film acts as an etch stop because the W film is not etched by the sequential exposures of BCl_3 and HF.

Figure 4 shows the WO_3 thickness versus number of BCl_3 and HF cycles at 207 °C for 20 cycles. The BCl_3 exposures were 325 mTorr s. The maximum BCl_3 pressure during these exposures was ~40 mTorr. The HF exposures were 200 mTorr

DOI: 10.1021/acsami.7b09161
ACS Appl. Mater. Interfaces 2017, 9, 34435−34447

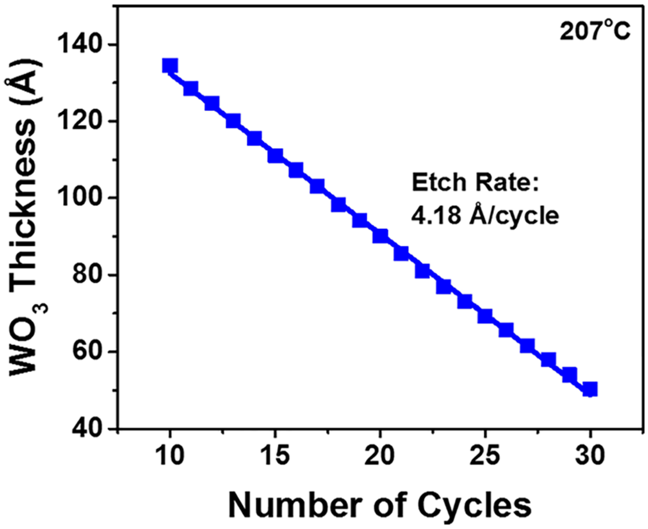

Figure 4. WO_3 thickness versus number of cycles showing WO_3 ALE at 207 °C using BCl_3 and HF as reactants. Etch rate during WO_3 ALE is 4.18 Å/cycle.

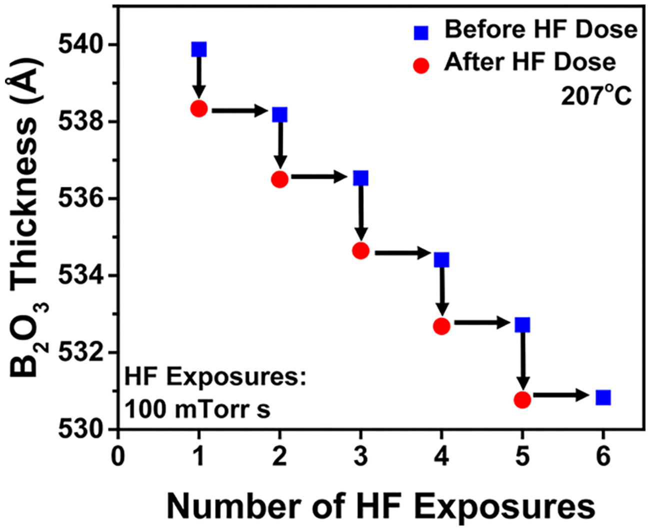

Figure 5. B_2O_3 thickness versus number of HF exposures showing spontaneous etching of B_2O_3 film at 207 °C. HF exposure was 100 mTorr s, and B_2O_3 etch rate is ∼2 Å per HF exposure.

s. The maximum HF pressure during these exposures was ∼60 mTorr. Each dose was followed by an UHP N_2 purge lasting 130 s. The data points in Figure 4 show the individual SE measurements of the WO_3 thickness after each reaction cycle. The etching of WO_3 is linear with an R^2 value of 0.999. The WO_3 etch rate is 4.18 Å/cycle. Multiple measurements of WO_3 ALE at 207 °C yielded etch rates that varied from 3.98−4.44 Å/cycle. Crystalline WO_3 has a monoclinic structure with cell dimensions of a = 7.306 Å, b = 7.540 Å, and c = 7.692 Å.[54] The WO_3 etch rate is slightly more than one-half of the WO_3 unit cell lengths.

The etching of WO_3 by BCl_3 and HF occurs by the "conversion-fluorination" mechanism where BCl_3 converts the WO_3 surface layer to a B_2O_3 layer. During the conversion of WO_3 to B_2O_3, the likely reaction product is a volatile WO_xCl_y compound. HF can then spontaneously remove the B_2O_3 layer by forming BF_3 and H_2O as reaction products. The removal of B_2O_3 regenerates the original WO_3 surface and completes one BCl_3/HF reaction cycle. The conversion of WO_3 to B_2O_3 is driven by the higher stability of B_2O_3 as compared to WO_3.[26] The etching of B_2O_3 by HF occurs because both BF_3 and H_2O are volatile reaction products.

To prove that B_2O_3 can be spontaneously etched by HF, B_2O_3 films were grown with BCl_3 and H_2O at 20 °C. This method was adapted from the previously reported B_2O_3 ALD process with BBr_3 and H_2O as the reactants at 20 °C.[55] B_2O_3 films were grown using 600 cycles of BCl_3 and H_2O at 20 °C. This B_2O_3 ALD process led to B_2O_3 films with a thickness of ∼580 Å. X-ray photoelectron spectroscopy (XPS) analysis of these films was consistent with stoichiometric B_2O_3 films. The B_2O_3 films were then heated to 207 °C for the HF exposures.

The B_2O_3 ALD films were exposed to HF pressures of 100 mTorr for 1 s. SE measurements were performed 60 s after the initial HF exposure. The SE measurements were then repeated 12 min after the first measurements to verify that no further etching occurred without additional HF exposures. Figure 5 shows the B_2O_3 film thickness versus the number of HF exposures for six HF exposures. Each HF exposure removes ∼2 Å of the B_2O_3 film. The second scan recorded after 12 min confirms that no additional etching is observed in the absence of HF exposures. These experiments demonstrate that HF can spontaneously etch the B_2O_3 film. The B_2O_3 etching is dependent on the HF pressure and the HF exposure time. The spontaneous B_2O_3 etching will continue for at least 20−30 HF exposures.

Both BCl_3 and HF exposures are required for WO_3 etching. Without HF exposures, BCl_3 exposures alone cannot etch WO_3. Without BCl_3 exposures, HF exposures alone did not etch WO_3. Figure 6 examines the self-limiting BCl_3 and HF reactions during WO_3 ALE at 207 °C. The etch rates were determined by varying one reactant while holding the other reactant at a constant reactant exposure. Each precursor was dosed into a stream of UHP N_2 gas at a pressure of 1180 mTorr. The purge time after each reactant exposure was 130 s.

The self-limiting behavior for the WO_3 etch rate versus the BCl_3 exposure is shown in Figure 6a. The BCl_3 exposures were varied from 0 to 492 mTorr s. The HF exposures were held constant at 200 mTorr s. Increasing the BCl_3 exposure to >225 mTorr s did not produce significantly more WO_3 etching. The BCl_3 reaction with WO_3 is self-limiting at the larger BCl_3 exposures with an etch rate of ∼4.2 Å/cycle.

The self-limiting behavior of the HF exposure is shown in Figure 6b. The HF exposure was varied from 0 to 318 mTorr s. BCl_3 exposures were held constant at 327 mTorr s. The WO_3 etch rate increases progressively versus HF exposure. Increasing the HF exposure to >200 mTorr s did not produce significantly more WO_3 etching. The HF reaction with WO_3 is self-limiting at larger HF exposures with an etch rate of ∼4.2 Å/cycle.

Figure 7 shows SE measurements that were recorded after each BCl_3 and HF exposure during WO_3 ALE at 207 °C for 26 half-cycles. The WO_3 thickness decreases linearly with the number of half-cycles. An expansion of the WO_3 thickness versus number of half-cycles for four half-cycles is displayed in Figure 8. The SE model assumed that the entire film was WO_3. Adding a Cauchy layer to account for the B_2O_3 layer on the WO_3 film after the BCl_3 conversion reaction did not improve the SE fitting. Figure 8 indicates that the WO_3 thickness etched in one BCl_3/HF cycle is 4.29 Å. The thickness loss after the BCl_3 exposure is 2.99 Å. The thickness loss after the HF exposure is 1.30 Å.

DOI: 10.1021/acsami.7b09161
ACS Appl. Mater. Interfaces 2017, 9, 34435−34447

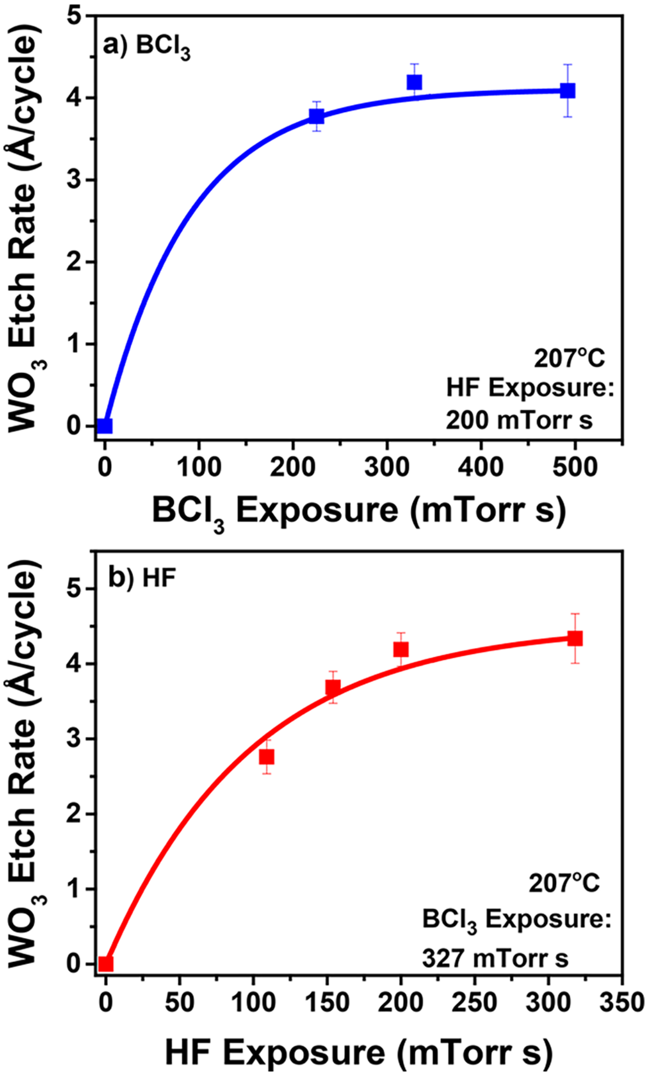

Figure 6. WO_3 etch rate versus reactant exposure during WO_3 ALE at 207 °C. (a) BCl_3 exposure was varied with HF exposure held at 200 mTorr s. (b) HF exposure was varied with BCl_3 exposure held at 327 mTorr s.

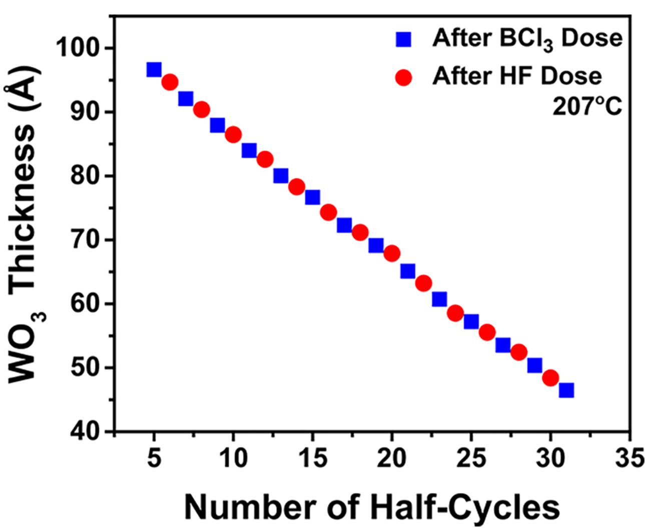

Figure 7. WO_3 thickness versus number of half-cycles during WO_3 ALE at 207 °C under self-limiting conditions.

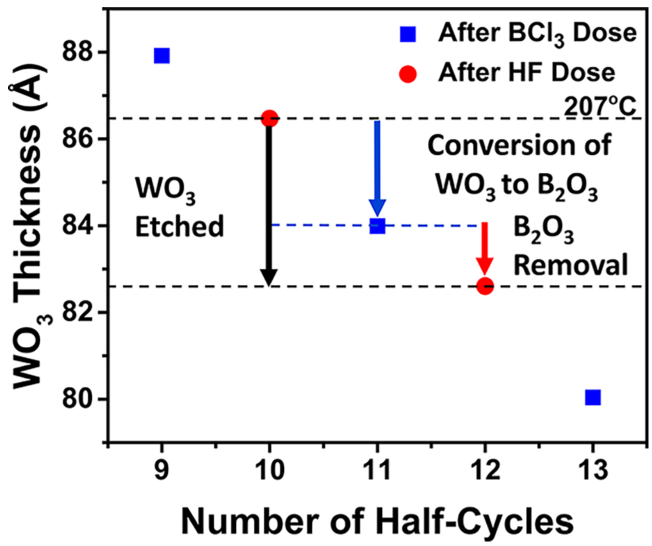

Figure 8. Analysis of WO_3 thickness change after BCl_3 exposure and HF exposure during WO_3 ALE at 207 °C.

The WO_3 thickness loss of 4.29 Å during one complete cycle represents 1.32×10^{-9} WO_3 mol/cm^2 based on a WO_3 density of 7.16 g/cm^3 and a WO_3 molar mass of 231.8 g/mol. During the WO_3 etching, WO_3 can be converted to various amounts of B_2O_3 depending on the possible BCl_3 conversion reactions given by eqs 3−5. The thickness loss of 2.99 Å after the BCl_3 exposure leaves a B_2O_3 thickness of 1.30 Å on the surface. The SE modeling assumes that the B_2O_3 thickness can be modeled as indistinguishable from a WO_3 thickness. This B_2O_3 thickness is then removed by the subsequent HF exposure.

The B_2O_3 thickness of 1.30 Å on the surface prior to removal by HF is in agreement with the BCl_3 conversion reaction given by eq 5. This BCl_3 conversion reaction yields WO_2Cl_2 as the volatile reaction product. On the basis of eq 5, the predicted B_2O_3 thickness remaining on the surface after the conversion of 4.29 Å of WO_3 or 1.32×10^{-9} WO_3 mol/cm^2 is 1.25 Å. The predicted B_2O_3 thickness of 1.25 Å agrees well with the measured B_2O_3 thickness of 1.30 Å. Mass spectrometry studies are needed to confirm WO_2Cl_2 as the volatile reaction product.

The WO_3 film thicknesses versus number of BCl_3 and HF reaction cycles at different substrate temperatures are shown in Figure 9. The self-limiting reaction conditions at 207 °C were used for all of the various temperatures. The self-limiting conditions were a BCl_3 exposure of 325 mTorr s and an HF exposure of 200 mTorr s. All of the initial WO_3 thicknesses were referenced to a starting value of 140 Å to compare the results at 128, 160, 196, and 207 °C. For all of the temperatures, the WO_3 etching is linear with the number of reaction cycles. The etch rate also increases at higher temperatures. The etch rates are 0.55, 2.04, 2.95, and 4.19 Å/cycle at 128, 160, 196, and 207 °C, respectively.

Figure 10 shows an Arrhenius plot of all of the etch rates at different temperatures acquired from the SE measurements. The approximately linear plot of ln(etch rate) versus $1/T$ shows that the etch rates are nearly exponentially dependent on temperature. The temperature-dependent WO_3 etch rate exhibits an activation energy of 8.6 kcal/mol. The temperature dependence of the WO_3 etch rate provides a means to control the WO_3 etch rate.

3.2. W ALE Using "Oxidation-Conversion-Fluorination" with O_3, BCl_3, and HF. The development of WO_3 ALE

DOI: 10.1021/acsami.7b09161
ACS Appl. Mater. Interfaces 2017, 9, 34435−34447

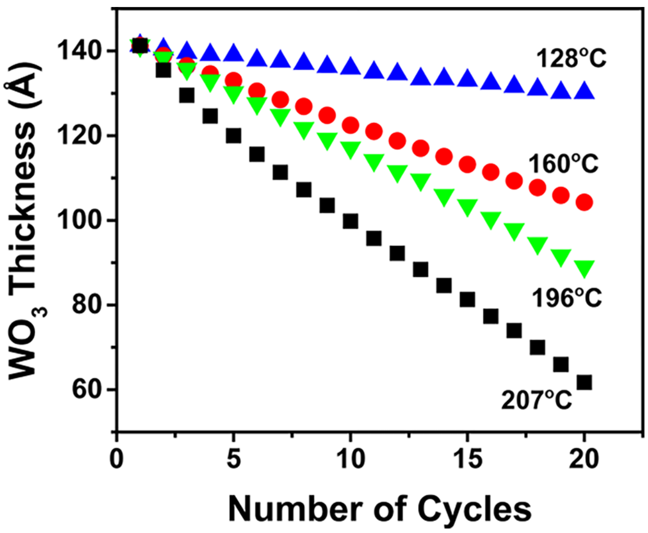

Figure 9. WO_3 thickness versus number of cycles for WO_3 ALE at 128, 160, 196, and 207 °C.

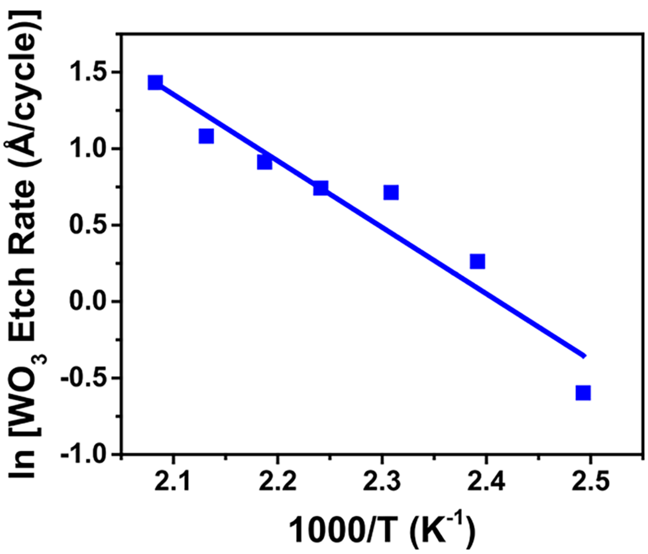

Figure 10. Arrhenius plot of temperature-dependent etch rates for WO_3 ALE. Slope of the Arrhenius plot yields an activation barrier of 8.6 kcal/mol.

opens a pathway to W ALE. Tungsten can first be oxidized to WO_3. Subsequently, WO_3 can be etched using sequential BCl_3 and HF exposures as described in section 3.1. The oxidation of W to produce WO_3 must be self-limiting to obtain atomic layer control of W etching. This requirement is demanding because oxidation of metals is generally very favorable, and often the oxidation can extend deep into the initial metal.

Tungsten oxidation has been studied extensively over a variety of temperatures and oxidation conditions. Many investigations have been reported at high temperatures >500 °C where tungsten oxidizes readily to form WO_3 and other tungsten oxides.[56,57] At temperatures >800 °C, these oxides can also desorb into the gas phase.[58] At temperatures between 300 and 400 °C, tungsten is oxidized by O_2 to form a WO_3 layer with thicknesses of 10−50 nm.[59−61] The WO_3 layer acts as a diffusion barrier that limits further oxidation.[62]

At lower temperatures of <300 °C, the tungsten oxidation is limited to thin WO_3 films on the W substrate.[59,61,63] Oxide thicknesses of 10−16 Å have been reported after O_2 exposures on polycrystalline W substrates for 1 h at 23−200 °C.[61] Somewhat thicker oxide thicknesses have been measured when using O_2 plasmas to oxidize tungsten at lower temperatures.[64,65] Tungsten oxidation at these lower temperatures is compatible with the temperature for WO_3 ALE and also is self-limiting at thin film thicknesses that are required for an ALE process.

Figure 11 shows results for the tungsten thickness versus number of ABC reaction cycles during W ALE at 207 °C. In

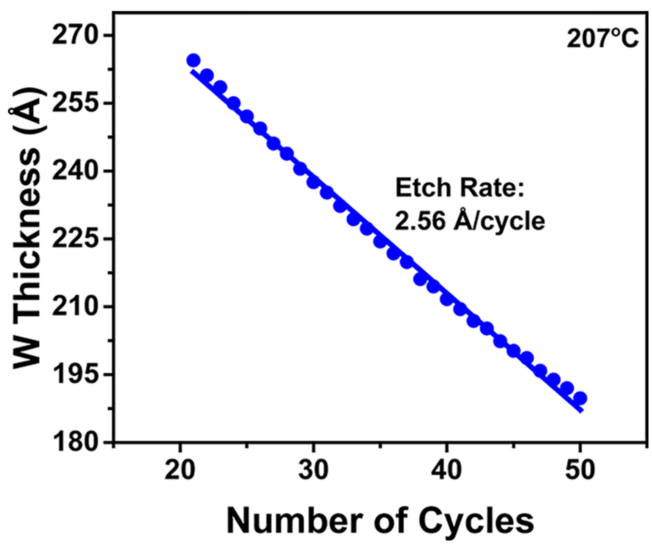

Figure 11. W thickness versus number of cycles during W ALE at 207 °C using O_2/O_3, BCl_3, and HF as reactants. Etch rate during W ALE is 2.56 Å/cycle.

these experiments, the surface of the W film was oxidized to WO_3 using O_2/O_3 pressures of 70 mTorr. The WO_3 layer was then etched using the next BCl_3 and HF exposures. The W ALE was conducted under self-limiting conditions for the O_2/O_3, BCl_3, and HF reactions at 207 °C as discussed below. The O_2/O_3 exposure was 3150 mTorr s, the BCl_3 exposure was 329 mTorr s, and the HF exposure was 2800 mTorr s.

Figure 11 reveals that the tungsten film thickness decreases linearly versus the number of cycles. The etch rate is 2.56 Å/cycle, and the R^2 value of the linear fit is 0.996. Multiple SE measurements of W ALE at 207 °C yielded etch rates that varied from 2.35−2.56 Å/cycle. XRR measurements confirmed the SE measurements. The W etch rate at 207 °C is slightly less than one unit cell length. W has a body-centered cubic structure with a unit cell length of 3.19 Å.

The WO_3 and W layer thicknesses could be determined simultaneously using SE measurements during W ALE. Figure 12 shows the concurrent SE measurements of the WO_3 and W film thicknesses versus the number of half-cycles at 207 °C. The half-cycles are the O_2/O_3 oxidation reaction and the BCl_3/HF etching reaction. The O_2/O_3 exposure was 3150 mTorr s, the BCl_3 exposure was 329 mTorr s, and the HF exposure was 2800 mTorr s. The ellipsometry measurements were performed after each half-cycle. The SE measurements were able to monitor both the growth and etching of the WO_3 layer and the concurrent removal of the underlying W film.

With an ABC exposure sequence, the WO_3 thickness is increased during W oxidization by O_2/O_3 and then decreased during the BCl_3 and HF etching reactions. The oxidation and

DOI: 10.1021/acsami.7b09161
ACS Appl. Mater. Interfaces 2017, 9, 34435−34447

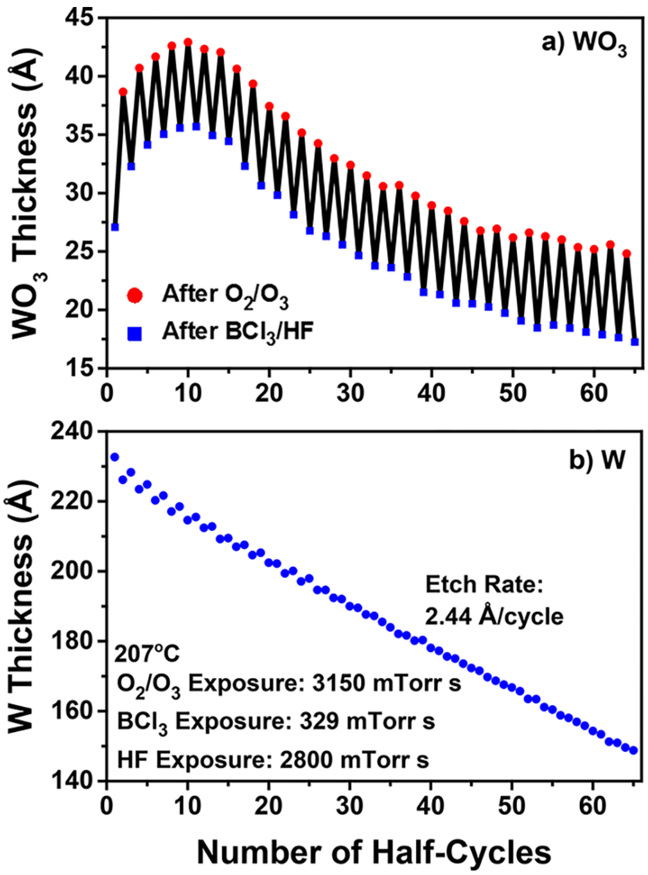

Figure 12. WO_3 and W thicknesses versus number of half-cycles during W ALE under self-limiting conditions using O_2/O_3, BCl_3, and HF as reactants at 207 °C. (a) WO_3 thickness showing oscillation of WO_3 thickness after O_2/O_3 exposure and BCl_3/HF reaction. (b) W thickness showing linear reduction versus number of half-cycles with an etch rate of 2.44 Å/cycle.

etching leads to an oscillatory WO_3 thickness in Figure 12a versus the number of half-cycles. The increase in the WO_3 thickness from oxidation is 7.2 Å/half-cycle averaged over five random half-cycles after 12 half-cycles. The decrease in the WO_3 thickness from the BCl_3/HF etching is 7.7 Å/half-cycle averaged over five random half-cycles after 12 half-cycles.

The WO_3 thickness loss of ~7.7 Å after the BCl_3/HF reactions during W ALE at 207 °C is larger than the WO_3 thickness loss of ~4.2 Å/cycle during WO_3 ALE at 207 °C. WO_3 ALE is performed with BCl_3 and HF as the reactants. W ALE is performed with O_2/O_3, BCl_3, and HF as the reactants. The addition of the O_2/O_3 exposure may alter the surface species and affect the BCl_3/HF reactions. Additional experiments were conducted where O_2/O_3 was removed from the ABC exposure sequence and WO_3 ALE was performed on WO_3 films produced using O_2/O_3. These experiments observed a WO_3 etch rate of ~4.2 Å/cycle that is the same as the etch rate of ~4.2 Å/cycle for WO_3 films produced using an O_2 plasma. The WO_3 etching is not dependent on the oxidant used to form the WO_3 film.

Figure 12a also observes an increase in the WO_3 thickness from ~30 to ~40 Å during the first 10 half-cycles. This increase is followed by a reduction to an oxide thickness of ~20 Å after 60 half-cycles. The change in the WO_3 thickness results from the competition between WO_3 growth during the O_2/O_3 exposures and WO_3 etching during the BCl_3/HF reactions. Higher or lower O_2/O_3 exposures were observed to result in more or less WO_3 growth. The presence of a maximum WO_3 thickness after 10 half-cycles in Figure 12a may be related to nucleation effects combined with the competition between WO_3 growth and WO_3 etching.

Concurrent ellipsometry measurements of the W thickness are shown in Figure 12b. While the WO_3 thickness is oscillating during the oxidation and etching half-cycles, the W thickness is reduced linearly versus number of half-cycles. The W etching rate is 2.44 Å/cycle. A small oscillation of the W thickness was observed over the first 30 half-cycles. The decreases in the W thickness during the half-cycles occur after the O_2/O_3 exposures when W is oxidized to WO_3. This slight oscillation may be an artifact from the ellipsometric modeling.

An expansion of the oscillation in the WO_3 thickness in Figure 12a is shown in Figure 13. The increase of the WO_3

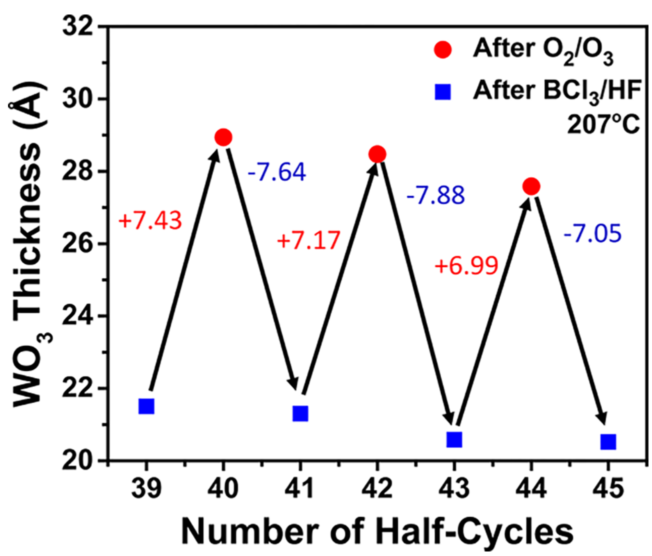

Figure 13. Enlargement of WO_3 thickness versus number of half-cycles showing increase and decrease of WO_3 thickness after O_2/O_3 exposure and BCl_3/HF reaction.

thickness during oxidation and the reduction of the WO_3 thickness during etching for six consecutive half-cycles are dramatic. Values of the individual WO_3 thickness increases and decreases are given in Figure 13. In addition, the increase in the WO_3 thickness from oxidation is 7.2 Å/half-cycle averaged over five random half-cycles after 12 half-cycles in Figure 12a. The decrease in the WO_3 thickness from the BCl_3/HF etching is 7.7 Å/half-cycle averaged over five random half-cycles after 12 half-cycles in Figure 12a.

The ratio of the WO_3 thickness gain per half-cycle and the W thickness loss per cycle should be equal to the ratio of the WO_3 and W molar volumes. This expectation is based on conservation of tungsten mass where a W loss must equal a WO_3 gain. The ratio of the WO_3 gain and W loss is 7.2 (Å/half-cycle)/2.44 (Å/cycle) = 2.95. In comparison, the ratio of the molar volumes for WO_3 and W is (32.4 cm^3/mol)/(9.5 cm^3/mol) = 3.4. The ratio of the molar volumes is only slightly higher than the ratio of the etch rates. This reasonable agreement is confirmation that W ALE occurs by conversion of W to WO_3 followed by the etching of WO_3. The slight differences in the ratios may also be explained by some WO_2 in the tungsten oxide layer. As compared to WO_3, WO_2 has a smaller molar volume of 20.0 cm^3/mol. The molar volume of a

DOI: 10.1021/acsami.7b09161
ACS Appl. Mater. Interfaces 2017, 9, 34435−34447

mixture of WO_3/WO_2 would lower the ratio of the molar volumes for WO_3/WO_2 and W.

The self-limiting nature of the O_2/O_3, BCl_3, and HF reactions is critical to establish a W ALE process. Self-limiting BCl_3 and HF reactions have already been established during the characterization of WO_3 ALE as shown in Figure 6. The self-limiting behavior of the O_2/O_3, BCl_3, and HF reactions during W ALE also needs to be verified to confirm a self-limiting procedure for W ALE.

Figure 14 displays the W etch rate versus O_2/O_3 exposure during the ABC reaction sequence at 207 °C. The pressure of the O_2/O_3 exposure was 70 mTorr for the different exposure times of 15, 30, 45, and 60 s. HF and BCl_3 exposures were held constant at 2800 and 500 mTorr s, respectively. The HF and BCl_3 pressures were 535 and 60 mTorr, respectively, during these exposures. Figure 14 shows that the W etch rate increases with O_2/O_3 exposure and reaches a maximum etch rate of 2.45 Å/cycle at an O_2/O_3 exposure of 3150 mTorr s. The line fitting the data points is meant to guide the eye.

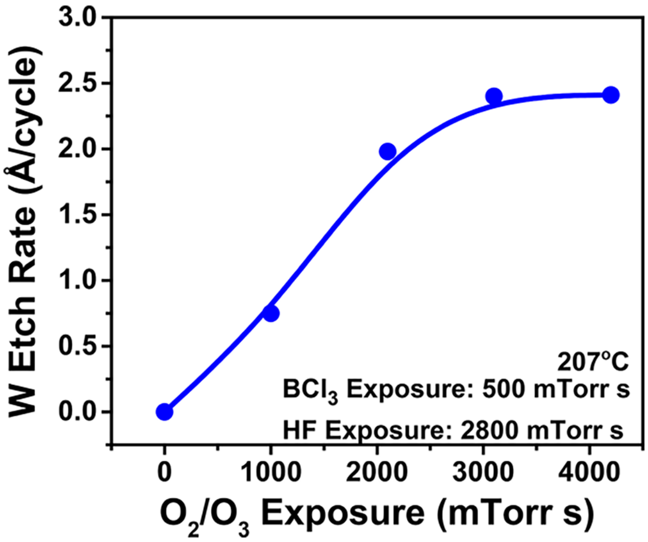

Figure 14. W etch rate versus O_2/O_3 exposure during W ALE at 207 °C. BCl_3 and HF exposures were held at 500 and 2800 mTorr s, respectively.

Results for the W etch rate versus BCl_3 or HF exposure during W ALE at 207 °C are shown in Figure 15a and b, respectively. These measurements were performed by varying one reactant exposure and holding the other two reactant exposures constant. BCl_3 and HF were dosed into a stream of UHP N_2 that was at a pressure of 1180 mTorr. A purge of 130 s was employed after each reactant exposure. The O_2/O_3 exposure was 3150 mTorr s conducted at an O_2/O_3 pressure of 70 mTorr. A purge of 60 s was used after each O_2/O_3 exposure.

Figure 15a shows the results for varying the BCl_3 exposure while holding the HF and O_2/O_3 exposures constant at 2800 and 3150 mTorr s, respectively. The BCl_3 exposures were varied from 0 to 500 mTorr s. The BCl_3 exposure converts the WO_3 surface to a B_2O_3 surface layer. The B_2O_3 surface layer is then spontaneously etched by HF. The W etch rate increases rapidly with BCl_3 exposure. With a BCl_3 exposure of 329 mTorr s, the W etch rate reaches the self-limiting W etch rate of 2.45 Å/cycle.

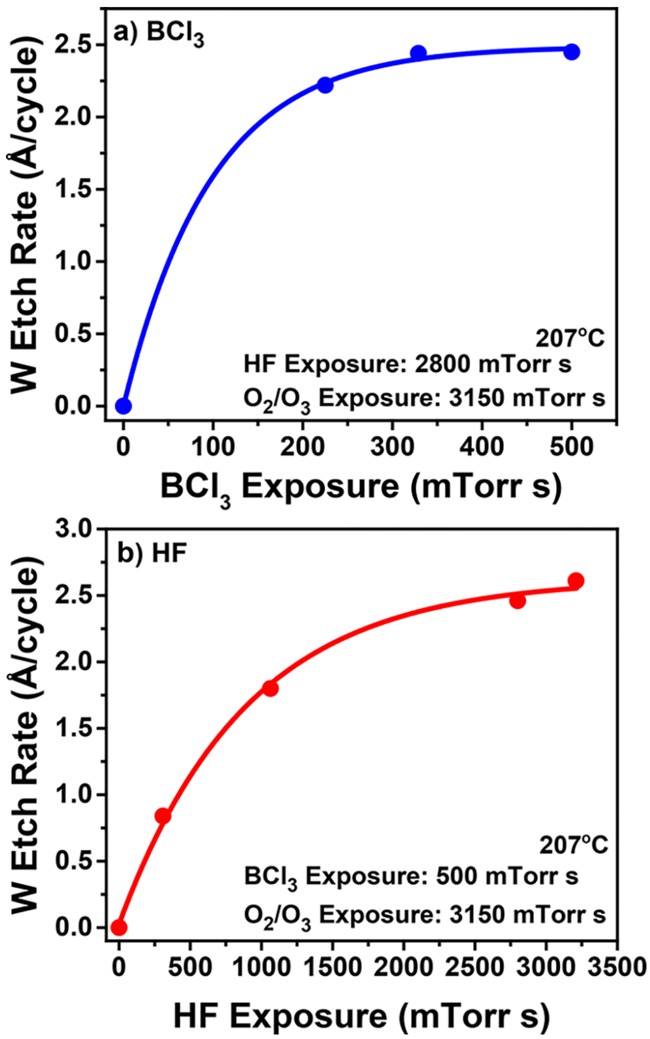

Figure 15. W etch rate versus reactant exposure during W ALE. (a) BCl_3 exposure was varied with HF and O_2/O_3 exposures held at 2800 and 3150 mTorr s, respectively. (b) HF exposure was varied with BCl_3 and O_2/O_3 exposures held at 500 and 3150 mTorr s, respectively.

Figure 15b shows the results for varying the HF exposure while holding the BCl_3 and O_2/O_3 exposures constant at 500 and 3150 mTorr s, respectively. Higher HF exposures progressively remove the B_2O_3 surface layer as volatile BF_3 and H_2O. With HF exposures of 2800 mTorr s, the W etch rate reaches the self-limiting W etch rate of 2.45 Å/cycle.

Additional experiments examined the oxidation of the W ALD films by successive O_2/O_3 exposures at 207 °C. The O_2/O_3 exposures were 3150 mTorr s resulting from an O_2/O_3 pressure of 70 mTorr for 45 s. This is the same O_2/O_3 exposure that was employed in the W ALE experiments. The W ALD films had been exposed to atmosphere prior to loading into the reactor. The WO_3 thickness on the W ALD film was then measured by SE after each O_2/O_3 exposure. The WO_3 thickness versus number of O_2/O_3 exposures is displayed in Figure 16.

The initial WO_3 thickness in Figure 16 is ~33 Å. This thickness is close to the native oxide thicknesses on tungsten that have been measured earlier with XPS and XRR analysis.[48,49] The WO_3 thickness is nearly constant at ~33 Å after the first three O_2/O_3 exposures. This constant oxide thickness may be related to the O_2/O_3 exposure cleaning

DOI: 10.1021/acsami.7b09161
ACS Appl. Mater. Interfaces 2017, 9, 34435−34447

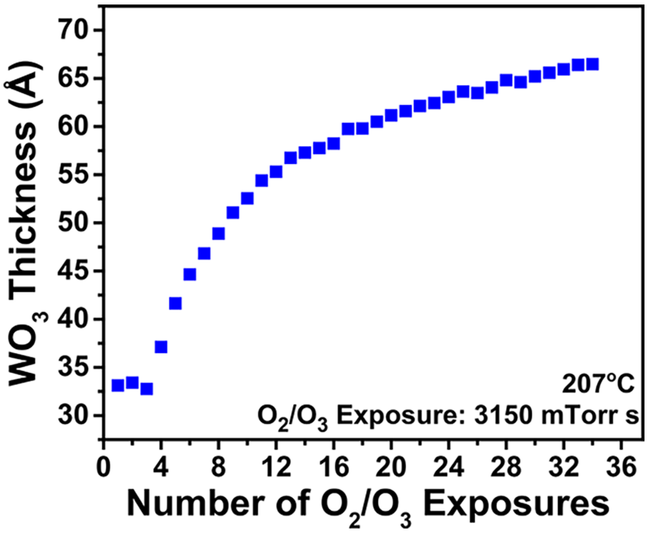

Figure 16. WO_3 thickness versus number of O_2/O_3 exposures for initial W ALD film. Each O_2/O_3 exposure was 70 mTorr for 45 s.

residual carbon from the surface. Figure 16 then shows that the WO_3 thickness increases consistently after the third O_2/O_3 exposure. However, the increase is progressively reduced after each O_2/O_3 exposure. This behavior is suggestive of diffusion-limited oxidation when the surface oxide acts as a barrier for oxidation of the underlying W metal. Similar behavior is also observed for the diffusion-limited oxidation of silicon described by the Deal–Grove model.[62] The WO_3 thickness is ~66 Å after 34 O_2/O_3 exposures. XPS analysis of the WO_3 film produced by these O_2/O_3 exposures was consistent with stoichiometric WO_3 with W in the 6+ oxidation state.

The larger WO_3 thicknesses produced by greater number of sequential O_2/O_3 exposures may lead to W etch rates that are higher after larger O_2/O_3 exposures. However, Figure 14 shows that the W etch rate is self-limiting versus O_2/O_3 exposure. This behavior suggests that the W ALE is self-limiting because of the self-limiting BCl_3 and HF reactions. Larger O_2/O_3 exposures may lead to larger WO_3 film thicknesses. However, the WO_3 removal is still limited by the self-limiting BCl_3 and HF reactions. The BCl_3 and HF reactions may only remove a fraction of the WO_3 film. After partial removal of the WO_3 film, the next O_2/O_3 exposure would then reestablish a larger WO_3 film thickness that is consistent with the O_2/O_3 exposure.

Additional experiments were performed at 207 °C by varying the O_2/O_3 exposure times with an O_2/O_3 pressure of 70 mTorr under self-limiting conditions for the BCl_3 and HF reactions. O_2/O_3 exposure times of 45 and 60 s both produced W ALE etch rates of 2.45 Å/cycle. However, the WO_3 film thickness was ~20 Å for the 45 s O_2/O_3 exposures (3150 mTorr s) and ~30 Å for the 60 s O_2/O_3 exposures (4200 mTorr s) after >20 reaction cycles. The consequence of larger O_2/O_3 exposure times at constant O_2/O_3 pressures is thicker WO_3 thicknesses during W ALE. However, the W ALE etch rates remain the same. These results argue that W ALE is self-limiting because of the self-limiting BCl_3 and HF reactions.

Figure 12a shows that the WO_3 thickness is reduced to a thickness of ~20 Å after 60 half-cycles during W ALE with an O_2/O_3 pressure of 70 mTorr and O_2/O_3 exposure time of 45 s under self-limiting conditions for the BCl_3 and HF reactions. Removal of this WO_3 layer on W may be important for applications where no oxide is desired for proper device function. This WO_3 layer can be removed by stopping the O_2/O_3 exposures and utilizing an AB reaction sequence with BCl_3 and HF exposures. Figure 17a displays the removal of the WO_3

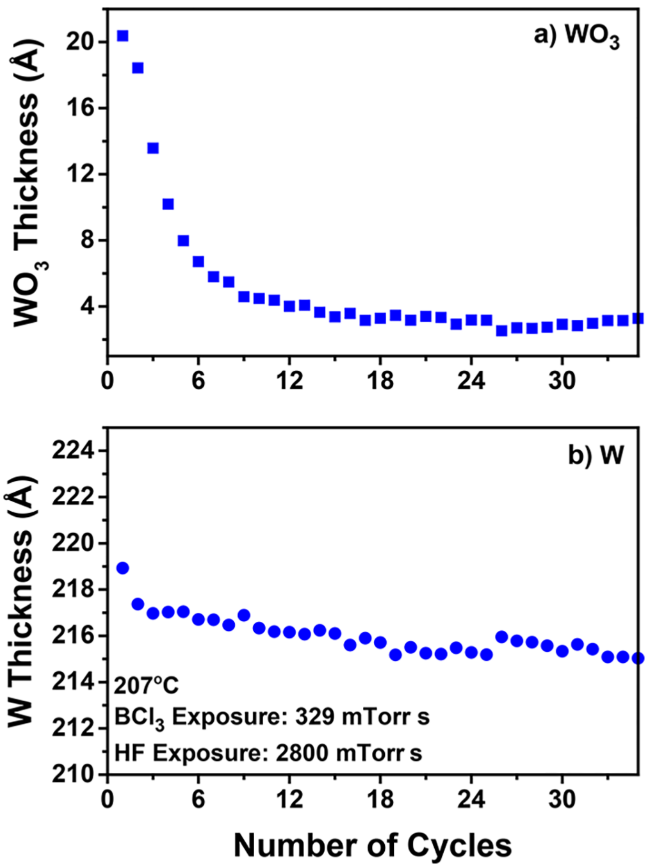

Figure 17. WO_3 removal after W ALE using BCl_3 and HF as reactants. (a) WO_3 thickness versus number of cycles showing reduction of WO_3 thickness to limiting value of ~3 Å. (b) W thickness versus number of cycles showing that W thickness remains nearly constant during WO_3 removal.

layer after W ALE versus the number of BCl_3/HF reaction cycles using the self-limiting reaction conditions for WO_3 ALE at 207 °C. The WO_3 layer thickness is reduced in thickness from 20 Å to a limiting thickness of ~3 Å after >12 reaction cycles.

The corresponding W film thickness during the removal of the WO_3 layer is shown in Figure 17b. While the WO_3 layer is removed during the AB reaction sequence, the W film thickness is nearly constant. The initial W film thickness is ~218 Å. The W film thickness reaches 215–216 Å after >12 reaction cycles. These results indicate that the WO_3 layer on W can be removed with almost no effect on the W thickness. There are also alternative methods to remove the WO_3 layer based on hydrogen reduction using H_2 or H_2 plasma exposures.[59,64,66]

The self-limiting conditions for the BCl_3 and HF exposures during WO_3 ALE at 207 °C were 325 and 200 mTorr s, respectively. In comparison, the self-limiting conditions for the O_2/O_3, BCl_3, and HF exposures during W ALE at 207 °C were 3150, 325, and 2800 mTorr s, respectively. The self-limiting conditions for the HF exposure are very different for WO_3 and W ALE. The inclusion of the O_2/O_3 exposure in the ABC reaction sequence for W ALE leads to a much larger self-limiting HF exposure. The chamber walls are coated with Al_2O_3

DOI: 10.1021/acsami.7b09161
ACS Appl. Mater. Interfaces 2017, 9, 34435−34447

ALD, and HF is known to adsorb on Al_2O_3 at the chamber wall temperature of 170 °C.[16] The O_2/O_3 exposure may remove HF from the chamber walls. Larger HF exposures may then be required during the subsequent BCl_3/HF reaction to replace the adsorbed HF and obtain self-limiting behavior.

3.3. Extension to Additional Materials. The "conversion-fluorination" and "oxidation-conversion-fluorination" mechanisms can be useful for the ALE of a variety of additional metal materials. These mechanisms will be valuable because some metal materials cannot be etched using the fluorination and ligand-exchange mechanism.[15,19] Fluorination of many metal materials is not thermodynamically favorable with HF. However, stronger fluorination reactants, like SF_4 and XeF_2, can lead to volatile metal fluorides and spontaneous etching. The highly exothermic reaction of stronger fluorination reagents with metal materials can also lead to fluoride layers too thick for ALE. Some metal materials are also difficult to fluorinate because they do not have stable fluorides in the same oxidation state as the initial metal material. Other metal materials can be fluorinated but do not easily yield volatile products during the ligand-exchange reaction.

BCl_3 is important for the conversion of many initial metal oxides to B_2O_3 because B_2O_3 is a stable metal oxide and many metals have volatile chlorides or oxychlorides. Metals with volatile chlorides or oxychlorides include W, V, Nb, Ta, Cr, Mo, Fe, Au, Ga, Ge, Sn, As, Sb, Zr and Hf. The spontaneous etching of B_2O_3 by HF also plays a key role in the new conversion etching mechanisms. HF can spontaneously etch B_2O_3. However, HF cannot spontaneously etch many other metal oxides. Consequently, if the initial metal oxide can be converted to B_2O_3, then HF can spontaneously etch B_2O_3 and the underlying initial metal oxide will serve as an etch stop.

Table 1 explores the thermochemistry of a variety of conversion reactions for various metal oxides. Most of these metal oxides will have difficulty achieving self-limiting ALE using fluorination and ligand-exchange reactions. The reasons for the difficulty include: (1) formation of volatile fluorides that lead to spontaneous etching (WO_3, MoO_3, VO_2, V_2O_5, Ta_2O_5, GeO_2, As_2O_3, Au_2O_3, SbO_2, Sb_2O_3, and NbO_2); (2) lack of volatile products after ligand-exchange reaction with various metal precursors (Fe_2O_3); and (3) absence of fluoride with the same oxidation state as the initial metal oxide (CrO_3). All of these metal oxides have volatile chlorides or oxychlorides and should be converted to B_2O_3 using BCl_3 based on thermochemical calculations. SnO_2, Ga_2O_3, ZrO_2, and HfO_2 ALE are possible using fluorination and ligand-exchange reactions.[20,21] These metal oxides are included in Table 1 because they have volatile chlorides or oxychlorides and could be etched using the "conversion-fluorination" mechanism as an alternative.

The thermochemistry of most of these reactions in Table 1 is favorable as measured by the standard free energy changes. The examples in Table 1 use either BCl_3 or $B(CH_3)_3$ for the conversion reaction to form B_2O_3. The choice of BCl_3 or $B(CH_3)_3$ depends on the volatility of the reaction products. In addition, the ligand on the boron center can also lead to selective ALE.[21] The thermochemical calculations reveal that Ga_2O_3 cannot be converted to B_2O_3 using $B(CH_3)_3$. Consequently, $B(CH_3)_3$ could be used to etch In_2O_3, GeO_2, As_2O_3, and SnO_2 without etching Ga_2O_3.

The conversion of metal oxides to other metal oxides besides B_2O_3 is also possible. One possibility is the conversion of metal oxides to TiO_2 using $TiCl_4$. Fluorination of TiO_2 using HF exposures would then spontaneously etch TiO_2 by producing volatile TiF_4 and H_2O reaction products.[67] $TiCl_4$ may not be as useful as BCl_3 for conversion etch. The thermochemistry of conversion of metal oxides to TiO_2 using $TiCl_4$ is not as favorable as the thermochemistry of conversion of metal oxides to B_2O_3 using BCl_3. However, the conversion of the surface of a metal oxide to a TiO_2 surface layer may be useful for device applications to avoid a TiO_2 ALD processing step.

Table 1. Thermochemistry of a Variety of Conversion Reactions for Various Metal Oxides

	$\Delta G°$ at 150 °C (kcal)
BCl_3 Conversion Reactions	
$As_2O_3 + 2BCl_3(g) \rightarrow B_2O_3 + 2AsCl_3(g)$	−81.3
$Au_2O_3 + 2BCl_3(g) \rightarrow B_2O_3 + 2AuCl_3(g)$	−134.5
$CrO_3 + 2/3BCl_3 \rightarrow 1/3B_2O_3 + CrO_2Cl_2(g)$	−93.7
$Fe_2O_3 + 2BCl_3(g) \rightarrow B_2O_3 + 2FeCl_3(g)$	−42.3
$Ga_2O_3 + 2BCl_3(g) \rightarrow B_2O_3 + 2GaCl_3(g)$	−61.6
$GeO_2 + 4/3BCl_3(g) \rightarrow 2/3B_2O_3 + GeCl_4(g)$	−76.7
$HfO_2 + 4/3BCl_3(g) \rightarrow 2/3B_2O_3 + HfCl_4(g)$	−15.6
$MoO_3 + 2/3BCl_3(g) \rightarrow 1/3B_2O_3 + MoO_2Cl_2(g)$	−19.1
$NbO_2 + 2/3BCl_3(g) \rightarrow 1/3B_2O_3 + NbCl_4(g)$	−13.6
$Sb_2O_3 + 2BCl_3(g) \rightarrow B_2O_3 + 2SbCl_3(g)$	−93.6
$SnO_2 + 4/3BCl_3(g) \rightarrow 2/3B_2O_3 + SnCl_4(g)$	−47.5
$Ta_2O_5 + 10/3BCl_3(g) \rightarrow 5/3B_2O_3 + 2TaCl_5(g)$	−42.8
$VO_2 + 4/3BCl_3(g) \rightarrow 2/3B_2O_3 + VCl_4(g)$	−26.0
$V_2O_5 + 2BCl_3(g) \rightarrow B_2O_3 + 2VOCl_3(g)$	−67.1
$ZrO_2 + 4/3BCl_3(g) \rightarrow 2/3B_2O_3 + ZrCl_4(g)$	−15.9
$TiCl_4$ Conversion Reactions	
$As_2O_3 + 3/2TiCl_4(g) \rightarrow 3/2TiO_2 + 2AsCl_3(g)$	−41.7
$CrO_3 + 1/2TiCl_4(g) \rightarrow 1/2TiO_2 + CrO_2Cl_2(g)$	−18.0
$Fe_2O_3 + 3/2TiCl_4(g) \rightarrow 3/2TiO_2 + 2FeCl_3(g)$	−2.7
$Ga_2O_3 + 3/2TiCl_4(g) \rightarrow 3/2TiO_2 + 2GaCl_3(g)$	−22.0
$GeO_2 + TiCl_4(g) \rightarrow TiO_2 + GeCl_4(g)$	−24.7
$MoO_3 + 1/2TiCl_4(g) \rightarrow 1/2TiO_2 + MoO_2Cl_2(g)$	−5.9
$Sb_2O_3 + 3/2TiCl_4(g) \rightarrow 3/2TiO_2 + 2SbCl_3(g)$	−54.0
$SnO_2 + TiCl_4(g) \rightarrow TiO_2 + SnCl_4(g)$	−21.1
$B(CH_3)_3$ Conversion Reactions	
$As_2O_3 + 2B(CH_3)_3(g) \rightarrow B_2O_3 + 2As(CH_3)_3(g)$	−83.0
$Ga_2O_3 + 2B(CH_3)_3(g) \rightarrow B_2O_3 + 2Ga(CH_3)_3(g)$	+34.1
$GeO_2 + 4/3B(CH_3)_3(g) \rightarrow 2/3B_2O_3 + Ge(CH_3)_4(g)$	−45.6
$In_2O_3 + 2B(CH_3)_3(g) \rightarrow B_2O_3 + 2In(CH_3)_3(g)$	−127.3
$SnO_2 + 4/3B(CH_3)_3(g) \rightarrow 2/3B_2O_3 + Sn(CH_3)_4(g)$	−26.8

4. CONCLUSIONS

The thermal ALE of WO_3 and W was demonstrated with new etching procedures using "conversion-fluorination" and "oxidation-conversion-fluorination" mechanisms. These procedures are important because earlier thermal ALE processes have utilized fluorination and ligand-exchange reactions that require the formation of a stable metal fluoride. In contrast, the new mechanisms are applicable for metal materials with volatile metal fluorides. Some elemental metals also require initial oxidation reactions because fluorination is very robust and leads to fluoride layers too thick for ALE.

The "conversion-fluorination" mechanism using an AB exposure sequence with BCl_3 and HF as the reactants was employed for WO_3 ALE. BCl_3 converts the WO_3 surface to a B_2O_3 layer and is believed to form volatile WO_2Cl_2 as a reaction product. The B_2O_3 layer is then spontaneously etched by HF to produce volatile BF_3 and H_2O. The BCl_3 and HF reactions

DOI: 10.1021/acsami.7b09161
ACS Appl. Mater. Interfaces 2017, 9, 34435−34447

were both self-limiting versus exposure. The WO_3 ALE etch rates were temperature dependent and increased from 0.55 Å/cycle at 128 °C to 4.19 Å/cycle at 207 °C. The W film acted as an etch stop because BCl_3 and HF could not etch the underlying W film.

The "oxidation-conversion-fluorination" mechanism using an ABC exposure sequence with O_2/O_3, BCl_3, and HF as the reactants was employed for W ALE. O_2/O_3 first oxidizes the W surface to a WO_3 layer. The WO_3 layer is then etched with BCl_3 and HF. The SE measurements could monitor simultaneously the W and WO_3 thicknesses during W ALE. The WO_3 thickness is oscillatory and increases during W oxidation and decreases during WO_3 etching. Concurrently, the W film thickness decreased linearly with number of ABC reaction cycles. W ALE was self-limiting with respect to each reaction in the ABC process. The etch rate for W ALE was ~2.5 Å/cycle at 207 °C. The residual WO_3 thickness of ~20 Å after W ALE could be removed with BCl_3 and HF reaction cycles without affecting the W layer.

These new etching mechanisms based on "conversion-fluorination" and "oxidation-conversion-fluorination" should be useful for the thermal ALE of a variety of materials. The conversion and fluorination reactions using BCl_3 and HF can be applied to many metal oxide materials including the oxides of W, V, Nb, Ta, Cr, Mo, Fe, Au, Ga, Ge, Sn, As, Sb, Zr, and Hf. The metals in these metal oxides can be converted to B_2O_3 by BCl_3 and have metal chlorides and metal oxychlorides that are volatile. The new "conversion-fluorination" and "oxidation-conversion-fluorination" mechanisms will be particularly valuable for providing ALE pathways for metals and metal oxides that have volatile metal fluorides.

AUTHOR INFORMATION

Corresponding Author

*E-mail: steven.george@colorado.edu.

ORCID

Steven M. George: 0000-0003-0253-9184

Notes

The authors declare no competing financial interest.

ACKNOWLEDGMENTS

This research was funded by the Semiconductor Research Corp. We thank Jonas Gertsch for depositing the initial W ALD films on the silicon wafers. We also acknowledge Advanced Energy in Fort Collins, CO, for the RF power supply and the impedance matching network for the ICP plasma source. In addition, we are grateful to Dr. Satyarth Suri of Intel Corp. for many useful discussions.

REFERENCES

(1) Carver, C. T.; Plombon, J. J.; Romero, P. E.; Suri, S.; Tronic, T. A.; Turkot, R. B. Atomic Layer Etching: An Industry Perspective. *ECS J. Solid State Sci. Technol.* **2015**, *4*, N5005−N5009.

(2) Faraz, T.; Roozeboom, F.; Knoops, H. C. M.; Kessels, W. M. M. Atomic Layer Etching: What Can We Learn from Atomic Layer Deposition? *ECS J. Solid State Sci. Technol.* **2015**, *4*, N5023−N5032.

(3) George, S. M. Atomic Layer Deposition: An Overview. *Chem. Rev.* **2010**, *110*, 111−131.

(4) Miikkulainen, V.; Leskela, M.; Ritala, M.; Puurunen, R. L. Crystallinity of Inorganic Films Grown by Atomic Layer Deposition: Overview and General Trends. *J. Appl. Phys.* **2013**, *113*, 021301.

(5) Kanarik, K. J.; Lill, T.; Hudson, E. A.; Sriraman, S.; Tan, S.; Marks, J.; Vahedi, V.; Gottscho, R. A. Overview of Atomic Layer Etching in the Semiconductor Industry. *J. Vac. Sci. Technol., A* **2015**, *33*, 020802.

(6) Athavale, S. D.; Economou, D. J. Realization of Atomic Layer Etching of Silicon. *J. Vac. Sci. Technol., B: Microelectron. Process. Phenom.* **1996**, *14*, 3702−3705.

(7) Park, S. D.; Lee, D. H.; Yeom, G. Y. Atomic Layer Etching of Si(100) and Si(111) Using Cl_2 and Ar Neutral Beam. *Electrochem. Solid-State Lett.* **2005**, *8*, C106−C109.

(8) Lim, W. S.; Park, S. D.; Park, B. J.; Yeom, G. Y. Atomic Layer Etching of (100)/(111) GaAs with Chlorine and Low Angle Forward Reflected Ne Neutral Beam. *Surf. Coat. Technol.* **2008**, *202*, 5701−5704.

(9) Park, S. D.; Oh, C. K.; Bae, J. W.; Yeom, G. Y.; Kim, T. W.; Song, J. I.; Jang, J. H. Atomic Layer Etching of InP Using a Low Angle Forward Reflected Ne Neutral Beam. *Appl. Phys. Lett.* **2006**, *89*, 043109.

(10) Metzler, D.; Bruce, R. L.; Engelmann, S.; Joseph, E. A.; Oehrlein, G. S. Fluorocarbon Assisted Atomic Layer Etching of SiO_2 using Cyclic Ar/C_4F_8 Plasma. *J. Vac. Sci. Technol., A* **2014**, *32*, 020603.

(11) Min, K. S.; Kang, S. H.; Kim, J. K.; Jhon, Y. I.; Jhon, M. S.; Yeom, G. Y. Atomic Layer Etching of Al_2O_3 Using BCl_3/Ar for the Interface Passivation Layer of III-V MOS Devices. *Microelectron. Eng.* **2013**, *110*, 457−460.

(12) Park, J. B.; Lim, W. S.; Park, B. J.; Park, I. H.; Kim, Y. W.; Yeom, G. Y. Atomic Layer Etching of Ultra-Thin HfO_2 Film for Gate Oxide in MOSFET Devices. *J. Phys. D: Appl. Phys.* **2009**, *42*, 055202.

(13) Kim, Y. Y.; Lim, W. S.; Park, J. B.; Yeom, G. Y. Layer by Layer Etching of the Highly Oriented Pyrolythic Graphite by Using Atomic Layer Etching. *J. Electrochem. Soc.* **2011**, *158*, D710−D714.

(14) Vogli, E.; Metzler, D.; Oehrlein, G. S. Feasibility of Atomic Layer Etching of Polymer Material Based on Sequential O_2 Exposure and Ar Low-Pressure Plasma-Etching. *Appl. Phys. Lett.* **2013**, *102*, 253105.

(15) George, S. M.; Lee, Y. Prospects for Thermal Atomic Layer Etching Using Sequential, Self-Limiting Fluorination and Ligand-Exchange Reactions. *ACS Nano* **2016**, *10*, 4889−4894.

(16) DuMont, J. W.; George, S. M. Competition Between Al_2O_3 Atomic Layer Etching and AlF_3 Atomic Layer Deposition Using Sequential Exposures of Trimethylaluminum and Hydrogen Fluoride. *J. Chem. Phys.* **2017**, *146*, 052819.

(17) Lee, Y.; DuMont, J. W.; George, S. M. Mechanism of Thermal Al_2O_3 Atomic Layer Etching Using Sequential Reactions with $Sn(acac)_2$ and HF. *Chem. Mater.* **2015**, *27*, 3648−3657.

(18) Lee, Y.; DuMont, J. W.; George, S. M. Trimethylaluminum as the Metal Precursor for the Atomic Layer Etching of Al_2O_3 Using Sequential, Self-Limiting Thermal Reactions. *Chem. Mater.* **2016**, *28*, 2994−3003.

(19) Lee, Y.; George, S. M. Atomic Layer Etching of Al_2O_3 Using Sequential, Self-Limiting Thermal Reactions with $Sn(acac)_2$ and HF. *ACS Nano* **2015**, *9*, 2061−2070.

(20) Lee, Y.; DuMont, J. W.; George, S. M. Atomic Layer Etching of HfO_2 Using Sequential, Self-Limiting Thermal Reactions with $Sn(acac)_2$ and HF. *ECS J. Solid State Sci. Technol.* **2015**, *4*, N5013−N5022.

(21) Lee, Y.; Huffman, C.; George, S. M. Selectivity in Thermal Atomic Layer Etching Using Sequential, Self-Limiting Fluorination and Ligand-Exchange Reactions. *Chem. Mater.* **2016**, *28*, 7657−7665.

(22) Johnson, N. R.; Sun, H.; Sharma, K.; George, S. M. Thermal Atomic Layer Etching of Crystalline Aluminum Nitride Using Sequential, Self-Limiting Hydrogen Fluoride and $Sn(acac)_2$ Reactions and Enhancement by H_2 and Ar Plasmas. *J. Vac. Sci. Technol., A* **2016**, *34*, 050603.

(23) Lee, Y.; DuMont, J. W.; George, S. M. Atomic Layer Etching of AlF_3 Using Sequential, Self-Limiting Thermal Reactions with $Sn(acac)_2$ and Hydrogen Fluoride. *J. Phys. Chem. C* **2015**, *119*, 25385−25393.

(24) DuMont, J. W.; Marquardt, A. E.; Cano, A. M.; George, S. M. Thermal Atomic Layer Etching of SiO_2 by a "Conversion-Etch" Mechanism Using Sequential Reactions of Trimethylaluminum and

DOI: 10.1021/acsami.7b09161
ACS Appl. Mater. Interfaces 2017, 9, 34435−34447

Hydrogen Fluoride. *ACS Appl. Mater. Interfaces* **2017**, *9*, 10296−10307.
(25) Zywotko, D. R.; George, S. M. Thermal Atomic Layer Etching of ZnO by a "Conversion-Etch" Mechanism Using Sequential Exposures of Hydrogen Fluoride and Trimethylaluminum. *Chem. Mater.* **2017**, *29*, 1183−1191.
(26) *HSC Chemistry*; HSC Chemistry 5.1, Outokumpu Research Oy: Pori, Finland.
(27) Adachi, S.; Susa, N. Reactive Ion Etching of Tungsten Films Sputter Deposited on GaAs. *J. Electrochem. Soc.* **1985**, *132*, 2980−2989.
(28) Morel, T.; Bamola, S.; Ramos, R.; Beaurain, A.; Pargon, E.; Joubert, O. Tungsten Metal Gate Etching in Cl_2/O_2 Inductively Coupled High Density Plasmas. *J. Vac. Sci. Technol. B* **2008**, *26*, 1875−1882.
(29) Tang, C. C.; Hess, D. W. Tungsten Etching in CF_4 and SF_6 Discharges. *J. Electrochem. Soc.* **1984**, *131*, 115−120.
(30) Balooch, M.; Fischl, D. S.; Olander, D. R.; Siekhaus, W. J. The Kinetics of Tungsten Etching by Atomic and Molecular Chlorine. *J. Electrochem. Soc.* **1988**, *135*, 2090−2095.
(31) Fischl, D. S.; Rodrigues, G. W.; Hess, D. W. Etching of Tungsten and Tungsten Silicide Films by Chlorine Atoms. *J. Electrochem. Soc.* **1988**, *135*, 2016−2019.
(32) Bensaoula, A.; Grossman, E.; Ignatiev, A. Etching of Tungsten with XeF_2 - An X-Ray Photoelectron Spectroscopy Study. *J. Appl. Phys.* **1987**, *62*, 4587−4590.
(33) Winters, H. F. The Etching of W(111) with XeF_2. *J. Vac. Sci. Technol., A* **1985**, *3*, 700−704.
(34) Blain, M. G.; Jarecki, R. L.; Simonson, R. J. Chemical Downstream Etching of Tungsten. *J. Vac. Sci. Technol., A* **1998**, *16*, 2115−2119.
(35) Peignon, M. C.; Cardinaud, C.; Turban, G. A Kinetic Study of Reactive Ion Etching of Tungsten in SF_6/O_2 Rf Plasmas. *J. Electrochem. Soc.* **1993**, *140*, 505−512.
(36) Schloh, M. O.; Leventis, N.; Wrighton, M. S. Microfabrication of WO_3-Based Microelectrochemical Devices. *J. Appl. Phys.* **1989**, *66*, 965−968.
(37) Strobel, A.; Schnabel, H. D.; Reinhold, U.; Rauer, S.; Neidhardt, A. Room Temperature Plasma Enhanced Atomic Layer Deposition for TiO_2 and WO_3 films. *J. Vac. Sci. Technol., A* **2016**, *34*, 01A118.
(38) Tagtstrom, P.; Martensson, P.; Jansson, U.; Carlsson, J. O. Atomic Layer Epitaxy of Tungsten Oxide Films Using Oxyfluorides as Metal Precursors. *J. Electrochem. Soc.* **1999**, *146*, 3139−3143.
(39) Hasper, A.; Holleman, J.; Middelhoek, J.; Kleijn, C. R.; Hoogendoorn, C. J. Modeling and Optimization of the Step Coverage of Tungsten LPCVD in Trences and Contact Holes. *J. Electrochem. Soc.* **1991**, *138*, 1728−1738.
(40) Kofuji, N.; Mori, M.; Nishida, T. Uniform Lateral Etching of Tungsten in Deep Trenches Utilizing Reaction-Limited NF_3 Plasma Process. *Jpn. J. Appl. Phys.* **2017**, *56*, 06hb05.
(41) Davidson, B. D.; Seghete, D.; George, S. M.; Bright, V. M. ALD Tungsten NEMS Switches and Tunneling Devices. *Sens. Actuators, A* **2011**, *166*, 269−276.
(42) Gray, J. M.; Houlton, J. P.; Gertsch, J. C.; Brown, J. J.; Rogers, C. T.; George, S. M.; Bright, V. M. Hemispherical Micro-Resonators from Atomic Layer Deposition. *J. Micromech. Microeng.* **2014**, *24*, 125028.
(43) Liu, R.; Lin, Y. J.; Chou, L. Y.; Sheehan, S. W.; He, W. S.; Zhang, F.; Hou, H. J. M.; Wang, D. W. Water Splitting by Tungsten Oxide Prepared by Atomic Layer Deposition and Decorated with an Oxygen-Evolving Catalyst. *Angew. Chem., Int. Ed.* **2011**, *50*, 499−502.
(44) Wetchakun, K.; Samerjai, T.; Tamaekong, N.; Liewhiran, C.; Siriwong, C.; Kruefu, V.; Wisitsoraat, A.; Tuantranont, A.; Phanichphant, S. Semiconducting Metal Oxides as Sensors for Environmentally Hazardous Gases. *Sens. Actuators, B* **2011**, *160*, 580−591.
(45) Hilfiker, J. N.; Singh, N.; Tiwald, T.; Convey, D.; Smith, S. M.; Baker, J. H.; Tompkins, H. G. Survey of methods to characterize thin absorbing films with Spectroscopic Ellipsometry. *Thin Solid Films* **2008**, *516*, 7979−7989.
(46) Wind, R. W.; Fabreguette, F. H.; Sechrist, Z. A.; George, S. M. Nucleation Period, Surface Roughness, and Oscillations in Mass Gain per Cycle during W Atomic Layer Deposition on Al_2O_3. *J. Appl. Phys.* **2009**, *105*, 074309.
(47) Klaus, J. W.; Ferro, S. J.; George, S. M. Atomic Layer Deposition of Tungsten Using Sequential Surface Chemistry with a Sacrificial Stripping Reaction. *Thin Solid Films* **2000**, *360*, 145−153.
(48) Wilson, C. A.; Goldstein, D. N.; McCormick, J. A.; Weimer, A. W.; George, S. M. Tungsten Atomic Layer Deposition on Cobalt Nanoparticles. *J. Vac. Sci. Technol., A* **2008**, *26*, 430−437.
(49) Wilson, C. A.; McCormick, J. A.; Cavanagh, A. S.; Goldstein, D. N.; Weimer, A. W.; George, S. M. Tungsten Atomic Layer Deposition on Polymers. *Thin Solid Films* **2008**, *516*, 6175−6185.
(50) Clancey, J. W.; Cavanagh, A. S.; Kukreja, R. S.; Kongkanand, A.; George, S. M. Atomic Layer Deposition of Ultrathin Platinum Films on Tungsten Atomic Layer Deposition Adhesion Layers: Application to High Surface Area Substrates. *J. Vac. Sci. Technol., A* **2015**, *33*, 01A130.
(51) Langereis, E.; Heil, S. B. S.; Knoops, H. C. M.; Keuning, W.; van de Sanden, M. C. M.; Kessels, W. M. M. In Situ Spectroscopic Ellipsometry as a Versatile Tool for Studying Atomic Layer Deposition. *J. Phys. D: Appl. Phys.* **2009**, *42*, 073001.
(52) Fijiwara, H. *Spectroscopic Ellipsometry: Principles and Applications*; John Wiley & Sons Ltd.: Hoboken, NJ, 2007.
(53) Johs, B.; Hale, J. S. Dielectric Function Representation by B-Splines. *Phys. Status Solidi A* **2008**, *205*, 715−719.
(54) Loopstra, B. O.; Rietveld, H. M. Further Refinement of Structure of WO_3. *Acta Crystallogr., Sect. B: Struct. Crystallogr. Cryst. Chem.* **1969**, *B 25*, 1420−1421.
(55) Putkonen, M.; Niinistö, L. Atomic Layer Deposition of B_2O_3 Thin Films at Room Temperature. *Thin Solid Films* **2006**, *514*, 145−149.
(56) Cifuentes, S. C.; Monge, M. A.; Perez, P. On the Oxidation Mechanism of Pure Tungsten in the Temperature Range 600−800 C. *Corros. Sci.* **2012**, *57*, 114−121.
(57) Gulbransen, E. A.; Andrew, K. F. Kinetics of the Oxidation of Pure Tungsten from 500 to 1300 C. *J. Electrochem. Soc.* **1960**, *107*, 619−628.
(58) King, D. A.; Madey, T. E.; Yates, J. T. Interaction of Oxygen with Polycrystalline Tungsten. 2. Corrosive Oxidation. *J. Chem. Phys.* **1971**, *55*, 3247−3253.
(59) Gulbransen, E. A.; Wysong, W. S. Thin Oxide Films on Tungsten. *Trans. Am. Inst. Min. Met. Eng.* **1948**, *175*, 611−627.
(60) Sohal, R.; Walczyk, C.; Zaumseil, P.; Wolansky, D.; Fox, A.; Tillack, B.; Mussig, H. J.; Schroeder, T. Thermal Oxidation of Chemical Vapour Deposited Tungsten Layers on Silicon Substrates for Embedded Non-Volatile Memory Application. *Thin Solid Films* **2009**, *517*, 4534−4539.
(61) Warren, A.; Nylund, A.; Olefjord, I. Oxidation of Tungsten and Tungsten Carbide in Dry and Humid Atmospheres. *Int. J. Refract. Hard Met.* **1996**, *14*, 345−353.
(62) Deal, B. E.; Grove, A. S. General Relationship for Thermal Oxidation of Silicon. *J. Appl. Phys.* **1965**, *36*, 3770−3778.
(63) King, D. A.; Madey, T. E.; Yates, J. T. Interaction of Oxygen with Polycrystalline Tungsten. 1. Sticking Probabilities and Desorption Spectra. *J. Chem. Phys.* **1971**, *55*, 3236−3246.
(64) Kim, J. K.; Nam, S. W.; Cho, S. I.; Jhon, M. S.; Min, K. S.; Kim, C. K.; Jung, H. B.; Yeom, G. Y. Study on the Oxidation and Reduction of Tungsten Surface for sub-50 nm Patterning Process. *J. Vac. Sci. Technol., A* **2012**, *30*, 061305.
(65) Romanyuk, A.; Melnik, V.; Oelhafen, P. Oxidation of Tungsten Surface with Reactive Oxygen Plasma. *Nucl. Instrum. Methods Phys. Res., Sect. B* **2005**, *232*, 358−361.
(66) Xu, S. L.; Diao, L. Study of Tungsten Oxidation in $O_2/H_2/N_2$ Downstream Plasma. *J. Vac. Sci. Technol., A* **2008**, *26*, 360−364.

(67) Lee, Y.; George, S. M. Thermal Atomic Layer Etching of Titanium Nitride Using Sequential, Self-Limiting Reactions: Oxidation to TiO_2 and Fluorination to Volatile TiF_4. *Chem. Mater.* **2017**, in press.

DOI: 10.1021/acsami.7b09161
ACS Appl. Mater. Interfaces 2017, 9, 34435−34447